ISSN 2070-0504, Catalysis in Industry, 2018, Vol. 10, No. 2, pp. 126–134. © Pleiades Publishing, Ltd., 2018.
Original Russian Text © O.P. Klenov, A.S. Noskov, O.A. Parakhin, 2017, published in Kataliz v Promyshlennosti.

ENGINEERING PROBLEMS. OPERATION AND PRODUCTION

Effect of the Density of a Microspherical Catalyst on the Operating Regimes of a Fluidized Bed

O. P. Klenov[a], *, A. S. Noskov[a], **, and O. A. Parakhin[b], ***

[a] *Boreskov Institute of Catalysis, Siberian Branch, Russian Academy of Sciences, Novosibirsk, 630090 Russia*
[b] *OOO NPO Sintez, Barnaul, 656015 Russia*
**e-mail: klen@catalysis.ru*
***e-mail: noskov@catalysis.ru*
****e-mail: office@cintez.org*

Received June 1, 2017

Abstract—An experimental study is performed of a circulating fluidized bed of two types of finely dispersed Geldart A particles with different bulk densities. The first type of particles have bulk density $\rho_b = 1200$ kg/m^3, while the bulk density of the second type of particles is $\rho_b = 1300$ kg/m^3. The studies are performed on a test bench 0.7 m in diameter and 5.75 m tall at room temperature with air used as the fluidizing gas. The velocity of fluidization ranges from 0.1 to 0.75 m/s. The bed is sectioned along its height with a set of horizontal diffuser grids. The results from measuring the fluctuations, the average drops in pressure, and the pressure distribution along the height of the fluidized bed are used to estimate the effect produced by the density of particles on its operational regimes. Velocity of transition U_c, determined from the mean-square deviations of pressure drop fluctuations, is 0.40 m/s for lighter particles and 0.35 m/s for heavier particles. Velocity of transition U_c determined from the power of the energy spectrum of pressure fluctuations E is 0.45 and 0.40 m/s for lighter and heavier particles, respectively. The results from pressure measurements along the bed height show a linear drop with increasing bed height, and this drop is faster for heavier particles than for lighter particles.

Keywords: fluidized bed, microspherical catalyst, turbulent regime, bed sectioning with horizontal grids, mean-square deviation of pressure drop fluctuations, particle bed density effect

DOI: 10.1134/S2070050418020101

INTRODUCTION

Catalytic processes in a circulating turbulent fluidized bed hold an important place in oil refining and petrochemical industries. This is exemplified by catalytic cracking, the synthesis of maleic anhydride, the dehydrogenation of C_3–C_5 paraffins, and so on [1–3].

These practical applications of a fluidized bed use finely dispersed catalyst particles that belong to class A of the standard Geldart classification [4]. This class is composed of particles with average diameter d_0 in the range of $40 < d_0 < 500$ μm and a specific density of the material of particles within a range of $1400 < \rho_0 < 4000$ kg/m^3. For spherical particles forming a fixed bed with a void fraction $\varepsilon_0 = 0.35$, this corresponds to the bulk density range of $910 < \rho_b < 2600$ kg/m^3.

The development of promising new types of catalysts for such processes and their industrial operation can create certain problems at existing plants. For example, the use of a new catalyst with a different specific density can change the pressure distribution and lead to the redistribution of a catalyst along the height of a reactor, even though the particle are characterized by the same patterns of their behavior during their gas fluidization, according to the classification within each class. To predict the changes in the technological regimes of industrial plants, we must have knowledge about the behavior of such systems upon a change in the physical parameters of a catalyst. This can be especially important when replacing a catalyst in reactors with internal devices designed for the distribution of particles along the height of a fluidized bed (e.g., in reactors sectioned with sets of diffuser grids along their height).

The main way of studying fluidized-bed systems is currently to perform experiments on test benches simulating certain characteristics of a real reactor.

Measurements and analysis of pressure fluctuations [5–13] and studies of the optical transmittance of local bed areas [14–16], which have gained wide acceptance due to the development of fiberoptic devices, are the main experimental means for studying a fluidized gas–solid bed. Capacitance sensors [8, 17] and the use of tracers [14] (e.g., radioisotope particles [18]) are more rarely applied. The use of pressure sensors for studying a fluidized bed was analyzed in [19].

The considerable number of works with experimental data on the use of pressure sensors for the diagnostics of a fluidized bed and the relative simplicity of measurements led us to choose this approach for this work.

It should be noted that the results from studies in all of the above works, and in the majority of literature sources, were obtained for a fluidized bed free of internal sectioning, distributing, heat-transfer, and other devices. Some general trends in the use of sectioning in a fluidized bed were described in [20]. Studies of louvered baffles were performed in [21, 22]. The use of X-rays to study a bubble regime with a single horizontal baffle simulating heat-transfer tubes was described in [23]. A gas tracer was used in [24] to study the mixing of a gas and solid particles in a model of a desorber with several rows of angular baffles. It was shown that both the design of baffles and the velocity of solid particle circulation affect the efficiency of desorption. Gas dispersion was found to be radially nonuniform; the maximum gas dispersion coefficient in the center was almost three times higher than near the desorber's wall.

The aim of this work was to study and compare the hydrodynamic characteristics of a circulating fluidized bed for catalyst particles of two types: ones that belong to the same Geldart class [4] but have different specific densities. The studies were performed on a large-scale test bench simulating the conditions in an industrial reactor with the use of air at room temperature as a fluidizing gas. Even though replacing such catalysts will not produce any qualitative changes in the operation of a fluidized-bed reactor, since they belong to the same class of bulk materials, this could lead to some quantitative changes in the hydrodynamic parameters. Estimates of the difference between the hydrodynamic regimes of different types of catalysts could therefore be useful for predicting the optimum technological regimes and controlling the flow for the operation of a process line.

EXPERIMENTAL

Hydrodynamic Test Bench

The scheme of the hydrodynamic test bench with a circulating fluidized bed is shown in Fig. 1. The main unit of this test bench is vertical cylindrical column *1* with a diameter of 0.7 m. The working section of this column is 5.75 m in height, and its total height is 7.15 m.

The catalyst bed is located in the working section of column *1* on non-sifting bubble-cap grid *2*. Flow inlet *3* into the column is located under grid *2* and equipped with a diffuser, which ensures a uniform flow distribution over the column's cross section at the inlet into the bed, together with bubble-cap grid *2*. The flow outlet from the column is designed in the form of three tubes *4* with diameters of 0.12 m, located in the horizontal plane at an angle of 90°. The two-stage purification system consists of three cyclones *5* and fine purification filters *6*, which can be shut off with drawers *7*. The hydraulic resistance of the filters is compensated for by fan *8* with flow rate controller *9*.

Catalyst circulation is ensured by three overflow tubes *10* of 0.05 m in diameter with expansion chambers *11* connecting cyclones *5* with column *1*. Chambers *11* are supplied with compressed air for the fluidization of the catalyst in the overflow tubes.

The air flow rate in column *1* is adjusted with reductor *12*, controlled with compressed air through secondary circuit *14*. The air flow rate is measured with measuring aperture *13*. Before being supplied into the column, air is moistened in vessel *15*, whose working section has a diameter of 0.4 m, to the relative humidity of 50–70%. To intensify mass transfer, the vessel is filled with packings of ceramic Raschig rings of $0.025 \times 0.025 \times 0.003$ m in size with a capacity of 0.1 m^3. Water is supplied to vessel *15* through valve *16* and distributed over the cross section with the diffuser device. A dehumidifier in the form of a package of pressed stainless steel chips is located under the packed bed. Water is periodically drawn out of the vessel through valve *17*. The relative air humidity is monitored with psychrometer *18*. The air flow rate in the column is additionally controlled with drawer *19*.

The pressure in the near-wall column area is measured through fittings *20* with a diameter of 5×10^{-3} m arranged on the column wall at a distance of 0.1 m from each other along the height. The fittings are equipped with porous filters to screen out microspherical particles of the studied catalyst. The filters are manufactured from TZMK-10 thermal protection material (quartz fibers). The selection of this material for the filters was dictated by its low hydrodynamic resistance ζ satisfying the condition $\varsigma = \dfrac{\Delta P_f}{0.5\rho_g U^2} < 300$ [17], in addition to its filtration properties.

Sectioning of a Fluidized Bed with Horizontal Diffuser Grids

Studies were performed for a fluidized bed sectioned with four horizontally installed diffuser grids along its height. Their structure is illustrated in Fig. 2. Grid layers were manufactured from steel angles of 0.05×0.004 m in size and arranged at distances of 0.4 m from one another along the height. The distance between the angles (the gap in the horizontal plane) is 0.032 m for the two upper layers (area A in Fig. 2) and 0.027 m for the two lower layers (area B). The dimensions of an angle as a major diffuser grid element, the arrangement of angles with respect to each other, and the distance between the layers of angles model the diffuser grid of an industrial reactor at a scale of 1 : 1.

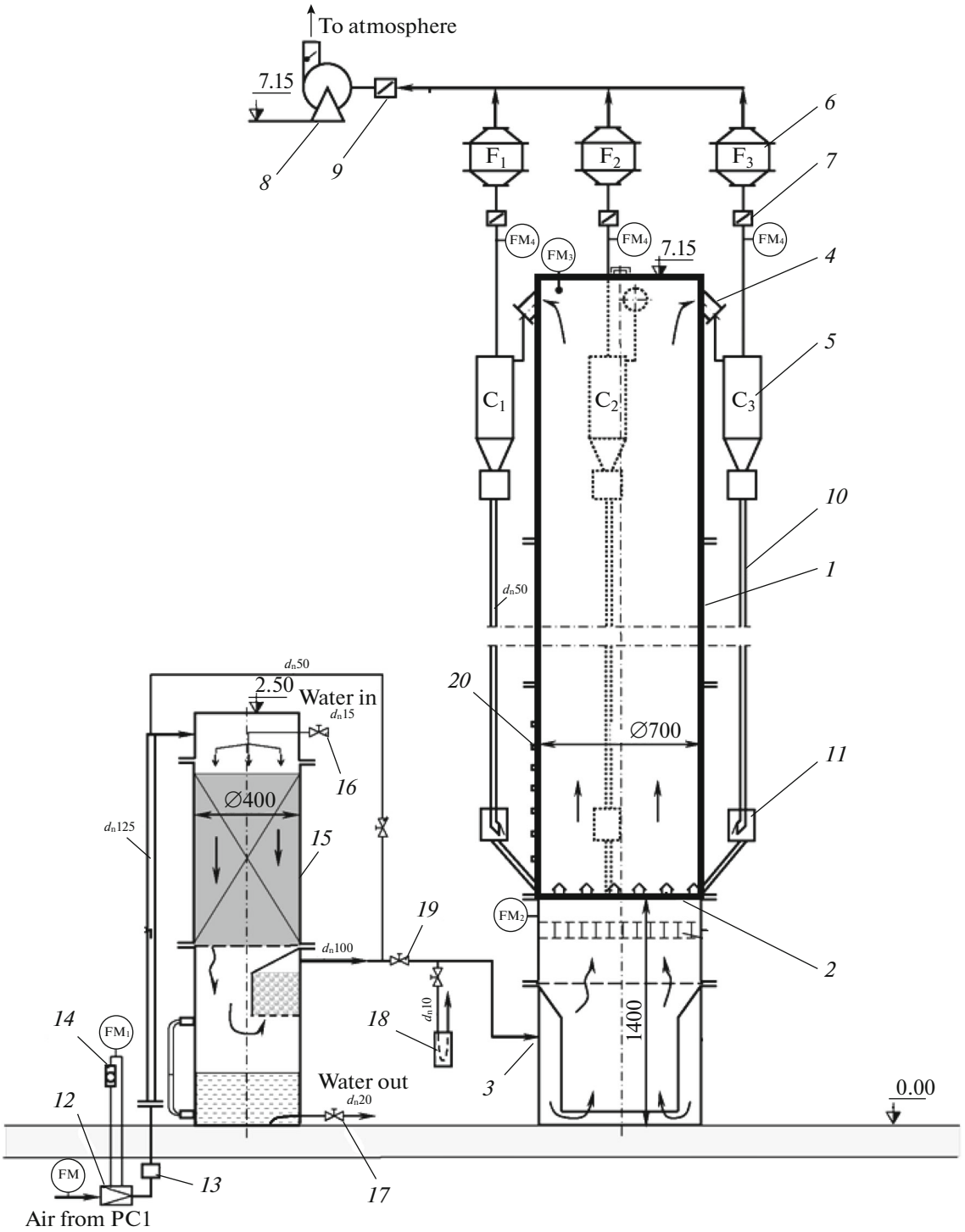

Fig. 1. Hydrodynamic test bench with a circulating fluidized bed.

The assembled grid was installed inside the column onto bubble-cap grid *2* (see Fig. 1).

Pressure Drop Measurement Points

Pressure drop measurement points on the column wall are shown in Fig. 3. The bed area between the measurement points incorporates the second lower diffuser grid and the free space over the first (lowermost) diffuser grid. The distances of 0.55 and 0.92 m to the pressure measurement points are counted from the bubble-cap grid on which the bed is located without fluidization. The height of the quiescent bed was $H_0 = 1.25$ m.

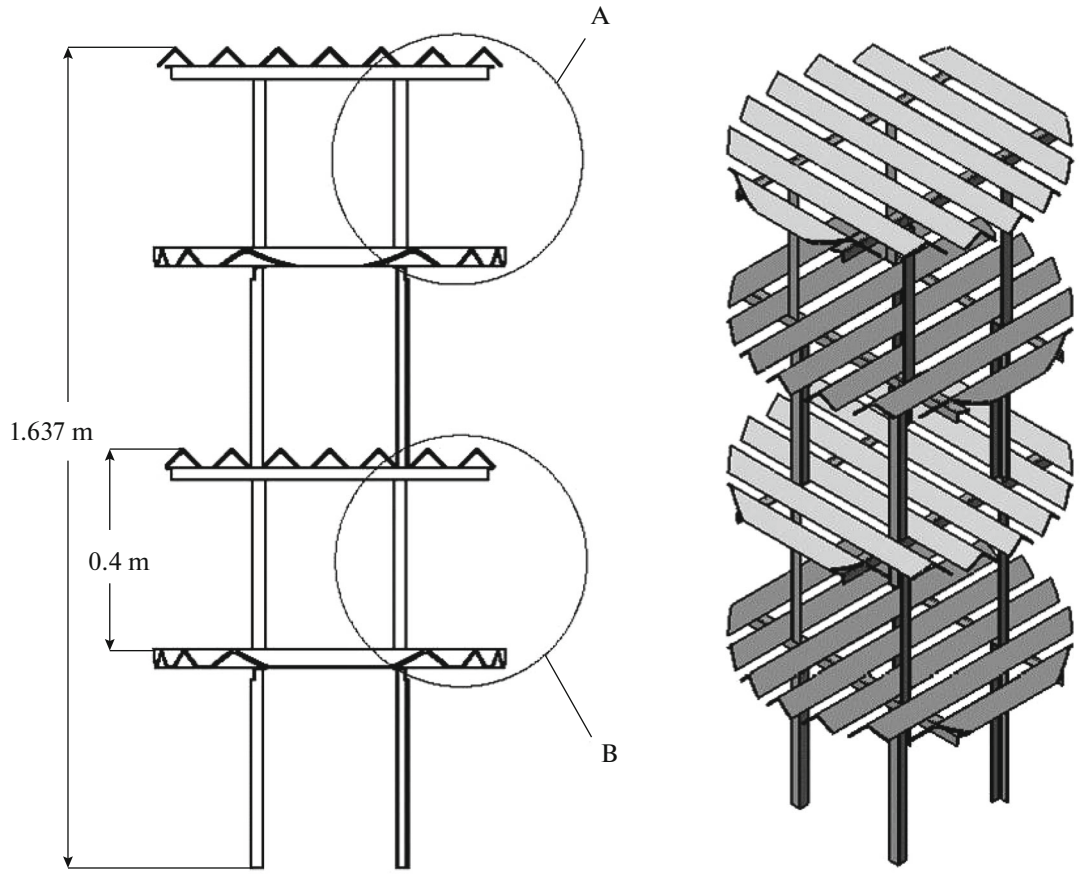

Fig. 2. Four-layer diffuser grid.

Studied Types of Catalyst Particles

Two types of microspherical catalyst particles with different specific densities were studied in this work. The selected characteristics of particles are given in Table 1.

These particles belong to class A of the Geldart classification [4], and the principal distinction between these two catalyst types with regard to the hydrodynamics of the formation and functioning of a fluidized bed in an industrial reactor is associated with their bulk density.

Measurement and Data Processing

Column pressure was measured with a device based on a Motorola MPX5010DP differential pressure sensor and equipped with a primary noise suppression system. It provided an outlet signal of up to $U_{max} = 0.5$ V upon a change in the medium's pressure drop within $\Delta P = 0–10.0$ kPa. The analog signal from this device was received by a NI9215 high-speed analog-to-digital converter with a NIUSB-9162 USB interface and connected to a personal computer.

The differential pressure sensor was calibrated using a TSI-1125 aerodynamic calibrator, a Testo526-2 digi-

Table 1. Selected characteristics of finely dispersed particles

Name	Type 1	Type 2
Bulk density ρ_b, kg/m^3	1200	1300
Average diameter of particles d_0, m	1.0×10^{-4}	1.0×10^{-4}
Particles with $d_0 < 7.0 \times 10^{-5}$ m, wt %	35	31
Particles with $7.0 \times 10^{-5} < d_0 < 1.4 \times 10^{-4}$ m, wt %	42	59
Particles with $d_0 > 1.4 \times 10^{-4}$ m, wt %	23	10

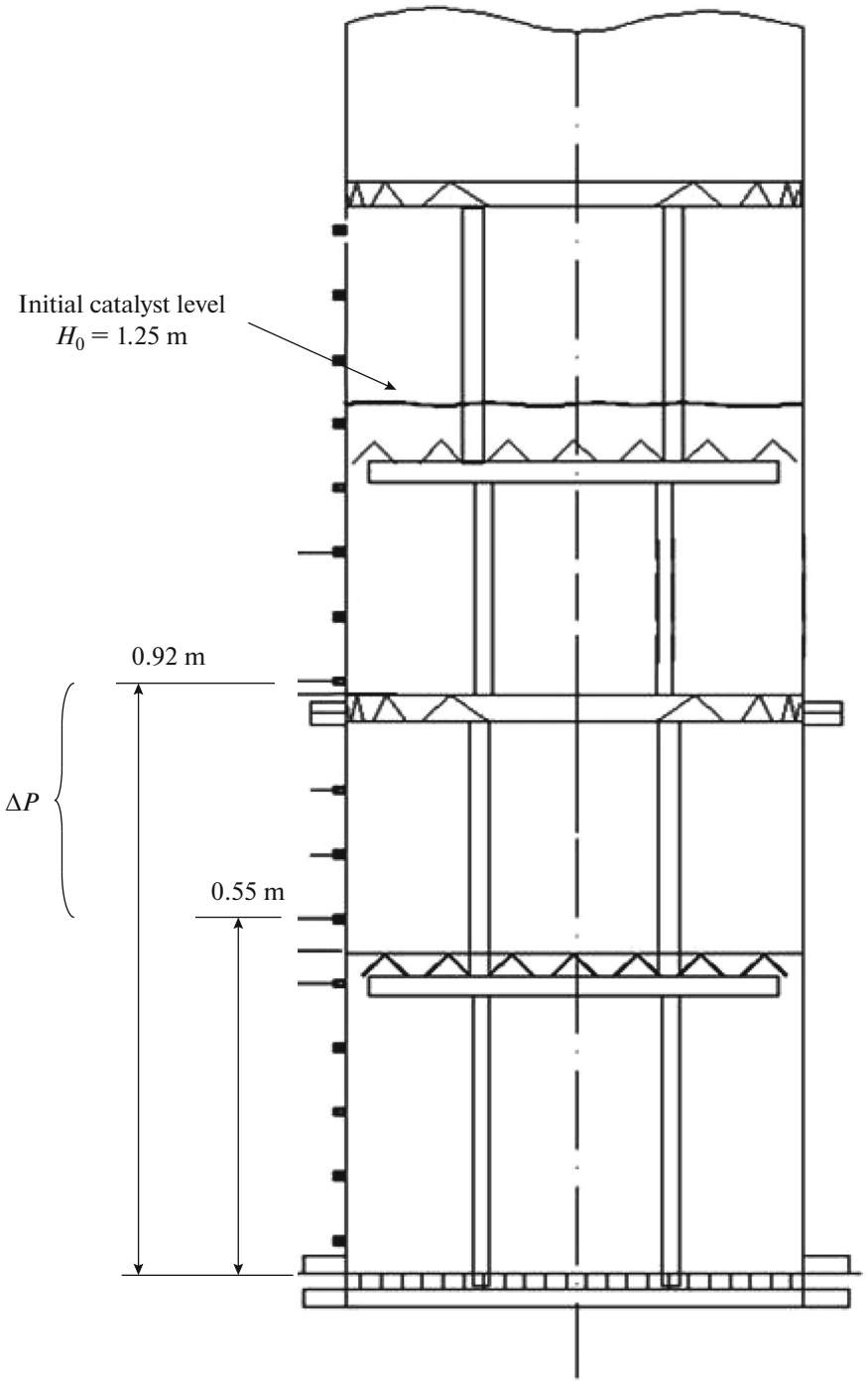

Fig. 3. Arrangement of points, at which the pressure drop ΔP was measured (the area comprises the second lower layer of the diffuser grid and the free space over the first (lowermost) diffuser grid).

tal pressure meter with an error of ±0.05%, and a MMH250 micro pressure gauge with an error of ±2.45 Pa. At low differential pressures ΔP ($0 < \Delta P \leq 35$ Pa), the relative measurement error ranged from +2.8 to −5.5%. The relative measurement error in the remaining differential pressure range $\Delta P > 35$ Pa was within ±0.8%.

The pressure drops in the fluidized bed were measured on the hydrodynamic test bench at different air velocities. The time τ_0 of each measurement was 25 s at step $\Delta\tau$ = 0.005 s. The array of data for each pressure drop measurement was then processed to determine the average values and mean-square deviations (MSDs). The frequency spectrum was found via fast Fourier transformation (FFT).

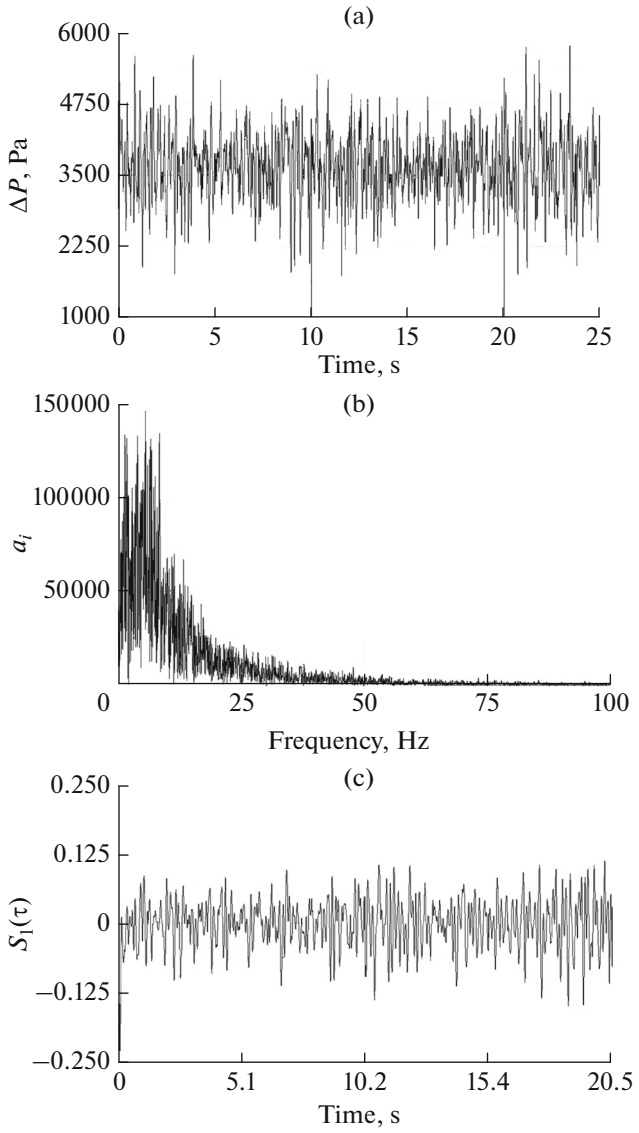

Fig. 4. (a) Pressure fluctuation $\Delta P(\tau)$ in the fluidized bed, (b) frequency $a_i = F(f)$ after Fourier transformation, and (c) self-correlation function $S_1(\tau)$ for the pressure fluctuation $\Delta P(\tau)$.

A typical differential pressure diagram is shown in Fig. 4a, and the frequency spectrum of this signal is illustrated in Fig. 4b. The self-correlation function was calculated for each measurement to determine the random character of the recorded signal. The self-correlation function of the signal shown Fig. 4a is plotted in Fig. 4c.

The frequency spectrum was analyzed as in [11, 12]. For each spectrum, the power of the energy spectrum of each signal E was calculated as [11]

$$E = \sqrt{\frac{\tau_0 \sum_i a_i^2}{N_{\text{FFT}}}}, \quad (1)$$

where $\tau_0 = 25$ s is the signal measurement time, N_{FFT} is the number of frequency range points for Fourier transformation (in this case, $N_{\text{FFT}} = 4096$), a_i is the signal spectrum amplitude for the ith value of frequency f. In our case, E was determined within frequency range $\Delta f = 0$–$f_{\max} = 100$ Hz.

The relative error in estimating power E was the error of pressure drop measurements and their analog-to-digital (ATD) conversion. As shown above, the relative pressure measurement error was within ±0.8%. The total relative ATD error was within ±0.05%, due to the finite number of digits and the nonlinear character of the ATD conversion function [25].

In addition, amplitude spectrum coefficient M was calculated as

$$M = 1 - \frac{f_m}{f_{\max}}, \quad (2)$$

where $f_{\max}$ is the maximum frequency ($\Delta f = 0$–$f_{\max}$ is the range of frequencies in which a signal is analyzed), and f_m is the frequency corresponding to the half-sum of signal amplitudes in selected range of frequencies Δf. In this work, the amplitude spectrum coefficient M was determined at two values of frequency window Δf: 30 Hz [12] and 100 Hz. The error in estimating coefficient M was due to the Fourier transformation frequency step, which in our case was $\delta = 0.024$ Hz. The error for frequency range $\Delta f = 30$ Hz was less than $\Delta M = \delta / f_{\max} = 0.08\%$.

RESULTS AND DISCUSSION

The results from calculating the mean-square deviation of pressure drop fluctuations ΔP at different bed fluidization velocities are shown in Fig. 5. Curve *1* corresponds to the interpolating function (the second-order polynomial that gives the best approximation reliability) for the lighter catalyst of type 1 with $\rho_b = 1200$ kg/m^3. Curve *2* corresponds to the catalyst of type 2 with $\rho_b = 1300$ kg/m^3.

The mean-square deviation of fluctuations for the heavier catalyst (type 2) is nearly 1.5 higher than for the particles of type 1 throughout the studied range of fluidization velocities W_o.

The dependences of the mean-square deviation on fluidization velocity W_o have an extremum with a maximum MDS corresponding to transition velocity U_c [11, 12]. Transition velocity U_c is an important characteristic of a fluidized bed and determines its transition to a turbulent regime when a substantial fraction of particles are lifted over the bed, i.e., the entrainment of catalyst particles from the bed begins [11]. Transition velocities U_c estimated from the mean-square deviation of pressure drop ΔP are close for both types of particles and lie within the range $0.35 \le U_c \le 0.40$ m/s.

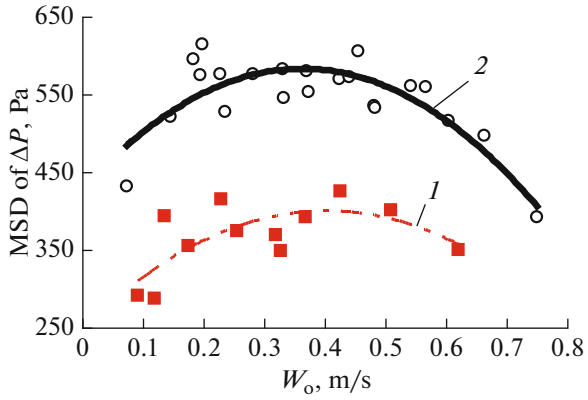

Fig. 5. Mean-square deviation of pressure drop fluctuations ΔP versus fluidization velocity W_o for both catalysts: particles of type (*1*) 1 and (*2*) 2.

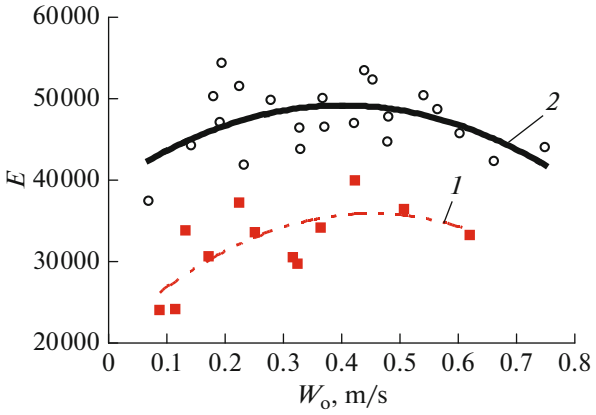

Fig. 6. Power E of the energy spectrum of pressure drop fluctuations ΔP versus fluidization velocity W_o for the particles of type (*1*) 1 and (*2*) 2.

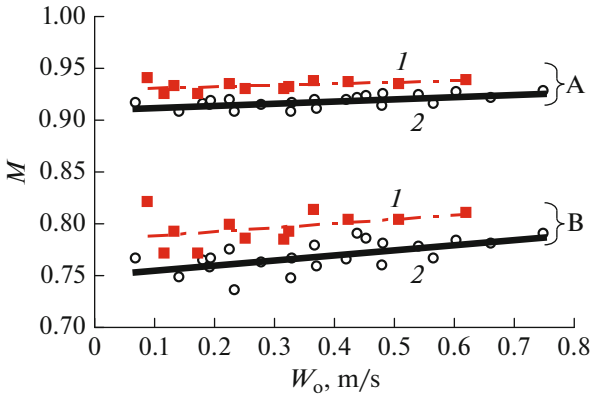

Fig. 7. Coefficeint M of the amplitude spectrum of pressure drop fluctuations ΔP versus fluidization velocity W_o within the frequency window Δf of (A) 100 and (B) 30 Hz for the particles of type (*1*) 1 and (*2*) 2.

The dependence of energy spectrum power E on fluidization velocity W_o for pressure drop fluctuations ΔP is plotted in Fig. 6. As in Fig. 5, curve *1* corresponds to the interpolation function for the lighter catalyst of type 1 with $\rho_b = 1200$ kg/m^3, and curve *2* corresponds to the catalyst of type 2 with $\rho_b = 1300$ kg/m^3.

The presented data on the power E of the spectrum of pressure drop fluctuations confirm the results obtained for the mean-square deviation of the amplitude of pressure drop fluctuations ΔP. The fluctuation spectrum power for the heavier particles of type 2 is nearly 1.44 times higher than for the lighter particles of type 1. The dependence of E on the fluidization velocity W_o has an extremum corresponding to the transition velocity U_c. The transition velocity determined from the plot for the fluctuation spectrum power is slightly higher than its value found from the plot of the mean-square deviation of pressure drop fluctuations and equal to 0.45 m/s for the particles of type 1 and 0.40 m/s for the particles of type 2.

The results from calculating of the amplitude spectrum coefficient M for the frequency ranges Δf of 100 and 30 Hz are shown in Fig. 7.

In contrast to the results for the mean-square deviation and the energy spectrum power E, the dependence of the amplitude spectrum coefficient M on the fluidization velocity is fitted best of all by a liner function. The absence of extremum points on the curve $M = F(W_o)$ does not allow us to determine the transition velocity U_c from the amplitude spectrum coefficient M; this distinguishing the obtained results from the known literature data. This could be due to the data shown in Fig. 7 being obtained for a fluidized bed structured along its height by diffuser devices, while most of the literature data were measured for a bed free of internal packings.

Coefficient M ranges within $0.9 < M < 0.95$ and $0.73 < M < 0.83$ for the processing of results within a frequency range $\Delta f = 100$ and 30 Hz, respectively. The value of M characterizes both the degree of spectrum dominance (i.e., the number of intense spectrum frequencies, and their arrangement with respect to the lower frequency window boundary f_{min}; in our case, $f_{min} = 0$). $M \cong 0.6$ corresponds to a uniform frequency intensity distribution over the entire spectrum within frequency range Δf, while $M \to 1.0$ corresponds to the spectrum with a single frequency, which is equal or close to f_{min}.

Coefficient M_1 for the lighter particles of type 1 is higher than M_2 for the heavier particles of type 2, i.e., $M_1 > M_2$ by 2–4% throughout the studied range of fluidization velocity W_o. This indicates the intensity of the frequency spectrum of turbulent fluctuations in the pressure drop for the particles of type 1 shifted by 2–4% toward lower frequencies, compared the particles of type 2.

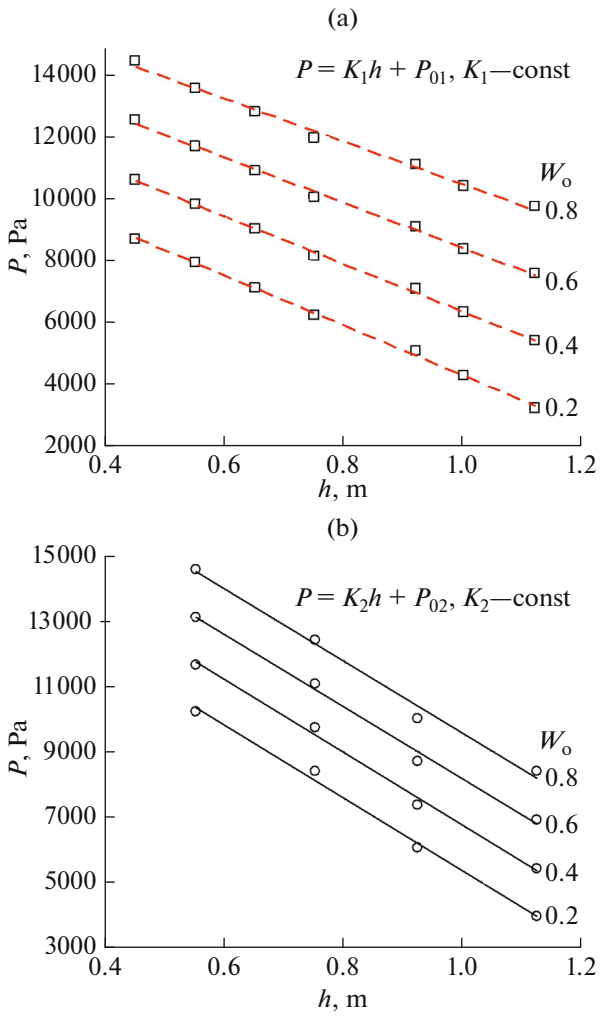

Fig. 8. Pressure distribution along the catalyst bed height at different fluidization velocities W_o for (a) the particles of type 1 with $\rho_b = 1200$ kg/m^3 and (b) the particles of type 2 with $\rho_b = 1300$ kg/m^3.

The distribution of pressure P along column height h for different fluidization velocities W_o is shown in Fig. 8. The dependence of the pressure on the column height can be fitted using a linear function with an approximation reliability R of $0.990 \le R^2 \le 0.999$.

Slope $K = \dfrac{dP}{dh}$ of curves $P(h) = Kh + P_0$ (i.e., the degree of reduction in pressure along the fluidized bed height) is nearly the same for every type of the studied particles. $K_1 = -7544.0$ Pa/m with mean-square deviation MSD$(K_1)/K_1 = 6.73\%$ for the particles of type 1, while $K_2 = -11140.8$ Pa/m with a mean-square deviation MSD $(K_2)/K_2 = 0.55\%$ for the particles of type 2.

Constant $P_0 = P(h = 0)$ depends on fluidization velocity W_o. From our results, it also follows that pressure P_0 at the bottom of the fluidized bed of the heavier particles of type 2 is nearly 24% higher than for the bed of the lighter particles of type 1 ($P_{02} > P_{01}$) at equal fluidization velocities W_o. The change in pressure P_0 upon a change in the density of particles ρ can be estimated using the empirical relation

$$P_{02} = P_{01}(\rho_2/\rho_1)^n, \quad (3)$$

where $n = 2.7$.

It should also be noted that the drop in pressure along the height of the bed formed of the heavier particles occurred more quickly than for the lighter particles ($K_1 < K_2$).

CONCLUSIONS

A turbulent fluidized bed sectioned along its height with a set of horizontal grids was studied experimentally for two types of particles belonging to class A of the Geldart classification with different bulk densities. The first type of particles had bulk density $\rho_b = 1200$ kg/m^3, while the bulk density for the second type was $\rho_b = 1300$ kg/m^3. The studies were performed on a cold test bench whose working unit was designed as a vertical column of 0.7 m in diameter and 5.75 m in height. Pressure drop fluctuations and average values and pressure distributions along the fluidized bed height were measured at fluidization velocity W_o ranging from 0.1 to 0.75 m/s.

The plots for the dependences of the mean-square deviation (MSD) of pressure drop fluctuations on fluidization velocity W_o were used to determine the transition velocity U_c for both types of particles. It was as high as 0.40 m/s for the lighter particles and 0.35 m/s for the heavier particles. These values were close to the ones found from the dependence of the energy spectrum power E on the fluidization velocity W_o, i.e., 0.45 and 0.40 m/s, respectively.

Amplitude spectrum coefficient M grew monotonically in the studied range of fluidization velocity W_o, rising from 0.1 to 0.8 m/s, and there were no extremum points for either type of the studied particles. Our results show that the intensity of the frequency spectrum of turbulent fluctuations in pressure drop ΔP for the particles of type 1 with $\rho_b = 1200$ kg/m^3 shifted by 2–4% toward lower frequencies, compared to the particles of type 2 with $\rho_b = 1300$ kg/m^3.

The results from pressure measurements along the bed height showed that the pressure fell linearly upon an increase in the bed height. The dependence of the pressure on the height can be described by a first-order polynomial in the form $P(h) = K_ih + P_{0i}$, where subscript i corresponds to the type of particles, K_i depends only on the type of particles, and pressure at the bed bottom P_{0i} depends on fluidization velocity W_o and the density of the particles. $K_1 = -7544.0$ Pa/m for the lighter particles of type 1, and $K_2 = -11140.8$ Pa/m for

the heavier particles of type 2. In other words, the drop in pressure along the bed height was faster for the heavier particles than for the lighter particles. At the same fluidization velocity W_o, the pressure at the bed bottom P_0 was higher for the heavier particles, and the change in P_0 upon a change in the density of particles can be estimated using the relation $P_{02} = P_{01}(\rho_2/\rho_1)^n$, where $n = 2.7$.

ACKNOWLEDGMENTS

This work was performed as a part of the state task for the Boreskov Institute of Catalysis of the Siberian Branch of the Russian Academy of Sciences (project no. 0303-2016-0010).

REFERENCES

1. Sadeghbeigi, R., *Fluid Catalytic Cracking Handbook,* Oxford: Elsevier, 2012.
2. Pakhomov, N.A., in *Promyshlennyi kataliz v lektsiyakh* (Industrial Catalysis in Lectures), Noskov, A.S., Ed., Moscow: Kalvis, 2006, vol. 6, pp. 53–98.
3. Sanfilippo, D. and Miracca, I., *Catal. Today,* 2006, vol. 111, nos. 1–2, pp. 133–139.
4. Geldart, D., *Powder Technol.,* 1973, vol. 7, no. 5, pp. 285–292.
5. Yerushalmi, J. and Cankurt, N.T., *Powder Technol.,* 1979, vol. 24, no. 2, pp. 187–205.
6. Baskakov, A.P., Tuponogov, V.G., and Filippovsky, N.F., *Powder Technol.,* 1986, vol. 45, no. 2, pp. 113–117.
7. Clark, N.N. and Atkinson, C.M., *Chem. Eng. Sci.,* 1988, vol. 43, no. 7, pp. 1547–1557.
8. Chehbouni, A., Chaouki, J., Guy, C., and Klvana, D., *Ind. Eng. Chem. Res.,* 1994, vol. 33, no. 8, pp. 1889–1896.
9. Bi, H.T., Grace, J.R., and Zhu, J., *Powder Technol.,* 1995, vol. 82, no. 3, pp. 239–253.
10. Bai, D., Shibuya, E., Masuda, Y., Nakagawa, N., and Kato, K., *Chem. Eng. Sci.,* 1996, vol. 51, no. 6, pp. 957–966.
11. Trnka, O., Veselý, V., Hartman, M., and Beran, Z., *AIChE J.,* 2000, vol. 46, no. 3, pp. 509–514.
12. Kashkin, V.N., Lakhmostov, V.S., Zolotarskii, I.A., Noskov, A.S., and Zhou, J.J., *Chem. Eng. J.,* 2003, vol. 91, nos. 2–3, pp. 215–218.
13. Johnsson, F., Zijerveld, R.C., Schouten, J.C., van den Bleek, C.M., and Leckner, B., *Int. J. Multiphase Flow,* 2000, vol. 26, no. 4, pp. 663–715.
14. Ege, P., Grislingås, A., and de Lasa, H.I., *Chem. Eng. J.,* 1996, vol. 61, no. 3, pp. 179–190.
15. Bai, D., Issangya, A.S., and Grace, J.R., *Ind. Eng. Chem. Res.,* 1999, vol. 38, no. 3, pp. 803–811.
16. Ellis, N., Briens, L.A., Grace, J.R., Bi., H.T. and Lim, C.J., *Chem. Eng. J.,* 2003, vol. 96, nos. 1–3, pp. 105–116.
17. Chen, A.H., Bi, H.T., and Grace, J.R., *Powder Technol.,* 2003, vols. 135–136, pp. 181–191.
18. Foka, M., Chaouki, J., Guy, C., and Klvana, D., *Chem. Eng. Sci.,* 1996, vol. 51, no. 5, pp. 713–723.
19. Bi, H.T. and Grace, J.R., *Chem. Eng. J. Biochem. Eng. J.,* 1995, vol. 57, no. 3, pp. 261–271.
20. Harrison, D. and Grace, J.R., in *Fluidization,* Davidson, J.F. and Harrison, D., Eds., New York: Academic Press, 1971, ch. 13.
21. Zhang, Y., Grace, J.R., Bi, X., Lu, C., and Shi, M., *Chem. Eng. Sci.,* 2009, vol. 64, no. 14, pp. 3270–3281.
22. Zhang, Y., Lu, C., and Shi, M., *Chem. Eng. Res. Des.,* 2009, vol. 87, no. 10, pp. 1400–1408.
23. Van Dijk, J.-J., Hoffmann, A.C., Cheesman, D., and Yates, J.G., *Powder Technol.,* 1998, vol. 98, no. 3, pp. 273–278.
24. Cui, H.P., Strabel, M., Rusnell, D., Bi, H.T., Mansaray, K., Grace, J.R., Lim, C.J., McKnight, C.A., and Bulbuc, D., *Chem. Eng. Sci.,* 2006, vol. 61, no. 2, pp. 388–396.
25. Serov, A.N., Development and study of an instrument for the increased-precision measurement of electric power quality characteristics, *Cand. Sci. (Eng.) Dissertation,* Moscow: Moscow Power Eng. Inst., 2016.

Translated by E. Glushachenkova